

Inductance of $\text{YBa}_2\text{Cu}_3\text{O}_{7-\delta}$ Thin-Films With and Without Superconducting Ground Planes

Han Cai , Hao Li , Ethan Y. Cho , and Shane A. Cybart , *Senior Member, IEEE*

Abstract—We experimentally measured and compared the sheet inductance of $\text{YBa}_2\text{Cu}_3\text{O}_{7-\delta}$ (YBCO) films with and without superconducting ground planes. Specifically, we fabricated several superconducting quantum interference devices from single and multilayer films with different geometries using a focused helium ion beam. Measurements of the device electrical transport properties were analyzed to determine the sheet inductance. Additionally, temperature dependent measurements of the inductance were used in order to separate the contributions from geometric and kinetic inductance. We found that the presence of a ground plane in our multilayer structure significantly reduces the contribution of the geometric inductance with no detectable change in the kinetic inductance.

Index Terms—Geometric inductance, ground plane, kinetic inductance, multilayer, $\text{YBa}_2\text{Cu}_3\text{O}_{7-\delta}$ (YBCO).

I. INTRODUCTION

SUPERCONDUCTING computing provides a promising high performance, energy-efficient alternative to conventional computing, where power and cooling for large-scale computing systems are drastically becoming unmanageable problems—especially for centralized supercomputers and data centers. With the advantages of wide temperature operation and low cost of cooling, high critical temperature (T_C) superconductors could revolutionize future systems. The computing speed and energy cost per bit of superconducting circuits depend strongly on their inductance. Therefore, critical factors affecting the performance of superconducting devices include precise design and control of the inductance. Additionally, technological improvements in the growth patterning and the interconnection of multiple layers can further optimize the inductance of more complex digital circuits [1]–[3].

Recent innovations in high-quality and reproducible $\text{YBa}_2\text{Cu}_3\text{O}_{7-\delta}$ (YBCO) devices fabricated by focused helium

Manuscript received December 28, 2019; revised May 7, 2020; accepted May 8, 2020. Date of publication June 3, 2020; date of current version July 6, 2020. This work was supported in part by the Air Force Office of Scientific Research under Grants FA955015-1-0218 and FA9550-17-1-0096, in part by the National Science Foundation under Grant 1664446, in part by the National Institutes of Health under Contract j1R43EB023147-01, in part by the University of California Office of the President, Multi-campus Research Programs and Initiatives under Award 009556-002, in part by UCOP MRPI under Grant MRP-17-454755, and in part by the Army Research Office under Grant W911NF1710504. This article was recommended by Associate Editor H. Rogalla. (*Corresponding author: Shane A. Cybart.*)

The authors are with the Department of Electrical and Computer Engineering, University of California, Riverside, Riverside, CA 92521 USA (e-mail: cybart@ucr.edu).

Color versions of one or more of the figures in this article are available online at <https://ieeexplore.ieee.org>.

Digital Object Identifier 10.1109/TASC.2020.2999390

ion beam focused helium ion beam (FHIB) irradiation[4]–[8] could aid in the development of high- T_C superconducting digital circuits. the beam energy of the FHIB is not high enough to penetrate thick films, unlike the prior-art of masked ion beam irradiated junctions [9]. Therefore, FHIB junctions are only suitable in the films with thicknesses much less than the penetration depth $\lambda_0 \sim 150$ nm [10]. This is particularly important because the inductance is dependant on the two-dimensional penetration depth, which rapidly increases with decreasing film thickness t , $\lambda_{\perp} = \lambda_L^2/t$.

In previous work [11]–[14], the total sheet inductance of YBCO can be reduced to just ~ 1 pH/□ with the addition of a ground plane. These demonstrations utilize 300 to 400 nm thick dielectric layers and 200 to 300 nm thick counter electrodes. In these structures, the film thicknesses are larger than their penetration depths. However, for films that are thinner than the material's penetration depth, the kinetic inductance dominates, meriting the study of the novel inductive properties of these materials. Therefore, in this article, we experimentally measured the geometric and kinetic inductance of commercially grown single and double layer YBCO thin films grown by reactive coevaporation [15] onto sapphire wafers with thicknesses much less than their penetration depth.

II. EXPERIMENT

Single and multilayer films of YBCO were grown on *r*-plane sapphire buffered with 20 nm of CeO_2 by Ceraco GmbH, with thicknesses much less than the penetration depth of YBCO. The single-layer film was 35-nm-thick. The multilayer structure consisted of two superconducting layers separated by an insulator with the following thicknesses: 35 nm YBCO, 75 nm CeO_2 , and 135 nm YBCO (from top to bottom). The insulating layer should be thick enough to prevent the leakage current from flowing through the pinholes in the CeO_2 . The total thickness needs to be kept to under 300 nm in order to ensure the film stability and to prevent cracking from happening during the deposition process. A 200-nm-thick gold electrode was evaporated *in situ* to make electrical contacts. In previous work, we detailed the synthesis of these multilayer films and verified that the two superconducting layers were isolated from one another with no pin-hole shorts through the CeO_2 insulator [16].

To investigate the sheet inductance (inductance per square), we utilized superconducting quantum interference devices (SQUIDs) with electrodes for direct current injection into the SQUID loop [17]. In these devices, inductance can be accurately

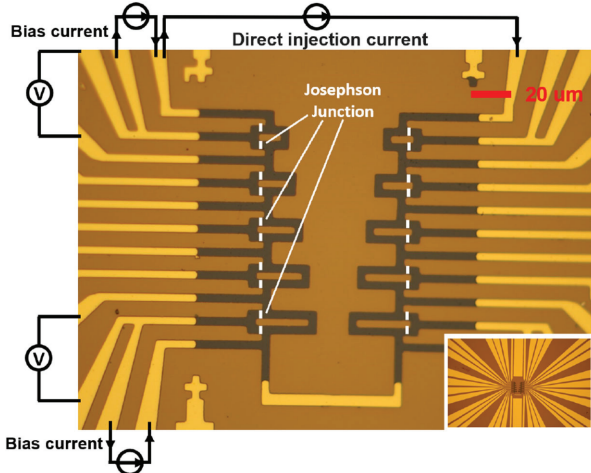


Fig. 1. Optical photograph of YBCO SQUIDS fabricated from the multilayer film. The center dark area is the exposed top YBCO pattern, where the gold electrode layer was chemically etched away. The solid white lines represent the Josephson junctions, which are directly written on the exposed top YBCO layer by the helium ion irradiation. The design is a symmetrical pattern, mirrored on either side of the center. From the top to the bottom, the direct control line follows the five SQUID loops that have 5, 7, 9, 11 and 13 squares of inductance.

determined by measuring the SQUIDS' magnetic field response to the injection current [18]. We fabricated several direct-inject SQUIDS in the upper layer of the multilayer sample as well as in a second single-layer sample using a fabrication method detailed in previous work [19], [20]. The multilayer SQUID chip is shown in Fig. 1. The area of the SQUID loop can be defined as the area of the largest single geometric square that can fit inside of the loop, times the number of those squares that make up the loop when the square is used to tile the geometric area. In our design, the SQUIDS have different areas of the loops with different numbers of squares: 5, 7, 9, 11, and 13, to accurately determine the sheet inductance of the material. The chips were created using laser lithography and argon ion milling in order to pattern the large-scale electrodes into both the gold and the top YBCO layer. In this situation, there is no return current flowing through the ground plane (the bottom YBCO layer). Therefore, the undesirable influence of the magnetic fields induced by the bias and the ground return currents can be neglected. Subsequently, Josephson junctions were written using a Zeiss Orion Plus helium ion microscope applying dosages of about $8 \times 10^{16} \text{ He}^+/\text{cm}^2$ to modify portions of the superconducting film into insulating lines that form Josephson junctions [4].

Completed devices were mounted in an evacuated dip probe and cooled in a liquid helium Dewar with magnetic shielding for electrical measurements. Each device was individually tested by dc biasing above the critical current (297.8 and 122.8 μA , respectively, for the single layer and multilayer SQUID at 4.2 K) and measuring the voltage–magnetic field (V – B) characteristics with an external magnetic field applied normal to the substrate from the backside of the sample. Fig. 2(a) shows the V – B plot for the single-layer device with a large modulation voltage amplitude of 135 μV . In contrast, Fig. 2(b) shows the multilayer device with no detectable modulation. This demonstrates that

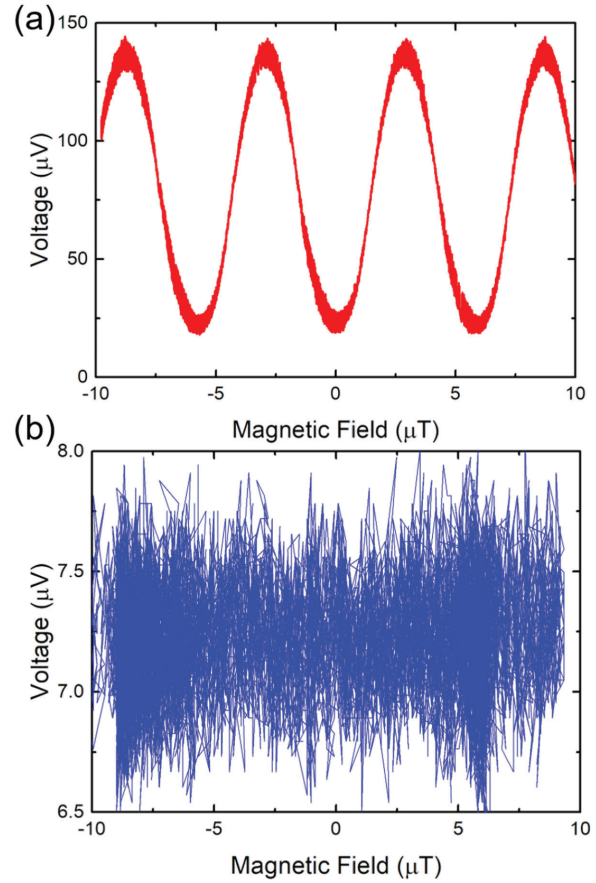


Fig. 2. Voltage external magnetic field characteristics for (a) single-layer thin film SQUID with 135 μV modulation amplitude and (b) SQUID on multilayer film with ground plane with no voltage-external magnetic field response.

the ground plane is superconducting and that it is sufficiently shielding the SQUIDS from the applied field.

Next, we measured the voltage response of the SQUID by injecting a current through the common injection line. The voltage modulation of the SQUIDS as a function of injection current (V – I_L) are shown in Fig. 3(a) and (b) for the single layer and for the multilayer, respectively. Both chips were operated over a large temperature range from 4 to 60 K. At 4.2 K, the modulation amplitudes were 60 μV for the single layer and 110 μV for the multilayer SQUID chip.

By comparing the magnetic field periods from the external field ΔB to the periodicity in current from the injection line I_L , we can accurately determine the injection inductance L_I and the sheet inductance $L_S = L_I/N$, where N is the number of squares of material. The inductance value of the SQUID loop is determined from $L = \Phi_0/\Delta B$. Using a linear fit shown in Fig. 4, the sheet inductance is obtained from the inductance plotted against the lengths of the square loops. At the lowest temperatures, we found L_S to be $6.2 \pm 0.2 \text{ pH}/\square$ and $4.3 \pm 0.4 \text{ pH}/\square$ for the single and multilayer films, respectively. This demonstrates that the ground plane in the multilayer device reduces the sheet inductance by almost a factor of two.

The thickness of the patterned YBCO layer (35 nm) is thin compared to the penetration depth of a magnetic field into

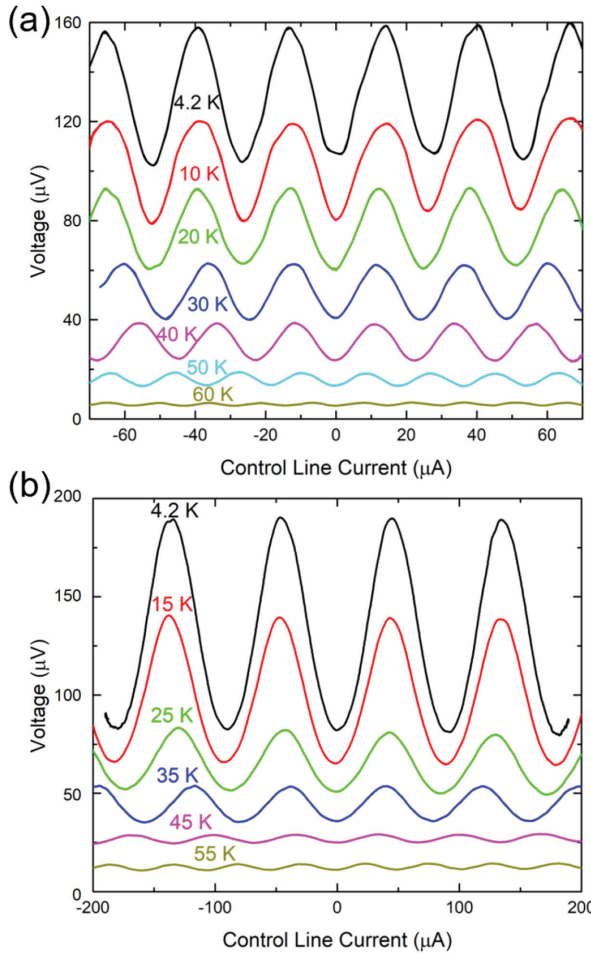


Fig. 3. Representative (a) single layer and (b) multilayer SQUID voltage—*injection current* characteristics (V — I_L) for several temperatures. The voltage modulation curves are all offsetting by $\sim 10 \mu\text{V}$ for clarity.

the superconductor. Because the film is sufficiently thin, the total inductance can be limited to only contributions from the kinetic and geometric inductance. To differentiate between the contributions from the geometric and kinetic inductance, we measured the dependence of the sheet inductance on temperature (see Fig. 5). The data are fitted using a model of d -wave superconductors with impurity scattering [21]–[23]

$$L_s = L_g + L_k(0)/[1 - (T/T_C)^2] \quad (1)$$

where L_g is the geometric inductance, L_k is the dependence of kinetic inductance on temperature, $L_k(0)$ is the value at 0 K, and T_C is the YBCO transition temperature. From a resistivity versus temperature measurement, we found the T_C taken at zero resistance for the single layer YBCO film, as well as for the top YBCO layer in the multilayer structure. The T_C values were found to be 79 K and 82 K, respectively.

Fig. 5 shows the dependence of inductance L_s on temperature was plotted against $[1 - (T/T_C)^2]^{-1}$, linearly fitted to (1). From the fit, we found the inductance properties of the single and multilayer devices. The geometric inductances L_g are $2.0 \pm 0.2 \text{ pH}/\square$ and $0.1 \pm 0.4 \text{ pH}/\square$, respectively, while the 0 K kinetic inductance L_k are $4.1 \pm 0.2 \text{ pH}/\square$ and $4.3 \pm 0.4 \text{ pH}/\square$.

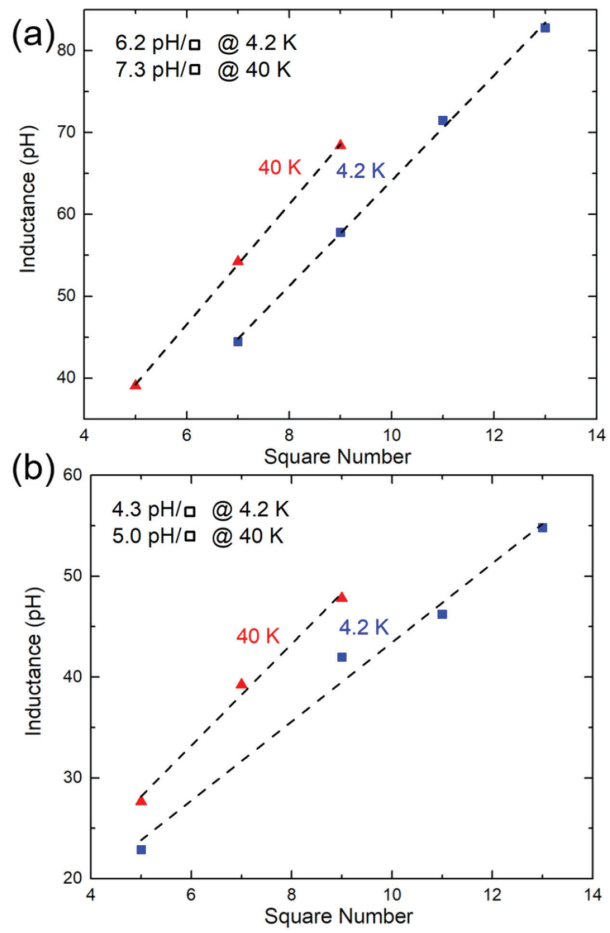


Fig. 4. Relationship of the number of squares in a SQUID loop versus the total inductance of that loop for (a) single and (b) multilayer films at high and low temperatures. The slope of the trend line gives the sheet inductance.

$\pm 0.4 \text{ pH}/\square$. As shown in Fig. 5, the geometric inductance of the multilayer is much smaller than that of the single-layer device, indicating that the ground plane can significantly reduce the contribution of the geometric inductance and effectively reduce the total sheet inductance with no detectable change in the kinetic inductance. As the geometric inductance refers to the magnetic energy stored within the film, the shielding effect from the ground plane is indicated by elimination of the geometric inductance. Moreover, the reduction of geometric inductance allows for higher operation frequencies in resultant devices.

The magnitude of the temperature dependent kinetic inductance is determined by the film thickness and is proportional to the penetration depth [24], $L_k/\square = \mu_0 \lambda(T)^2/t$, where $\lambda(T) = \lambda(0)/\sqrt{[1 - (T/T_C)^2]}$. The kinetic inductance becomes constant when there is no change in the penetration depth at low temperatures. For the inductance of the multilayer device, the kinetic inductance dominates, which leads to the inductance becoming constant at low temperatures. It is also responsible for the appearance of an upturn in the plot of Fig. 5(b) at low temperatures. From the kinetic inductance, the penetration depth can be estimated to be about 290 nm. However, the calculated penetration depth may be larger than the actual value due to uncertainties in the film thickness measurement.

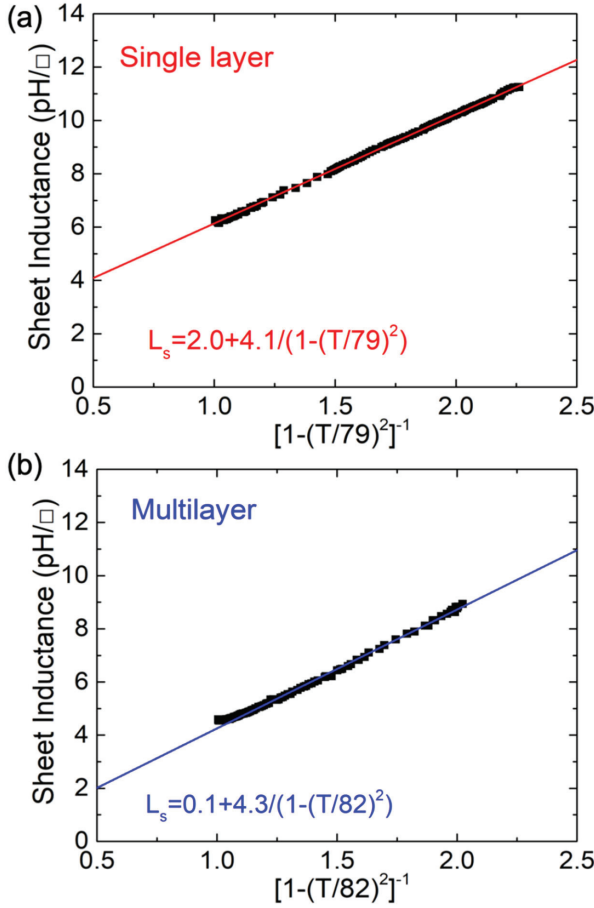


Fig. 5. Relationship between inductance L_s and $[1 - (T/T_c)^2]^{-1}$. Black squares are the measurement data. The solid curve is the result of the fit.

The kinetic inductance responds to the superconducting state and the nondissipative kinetic energy of the supercurrent [25]. The addition of a ground plane does not induce more energy dissipation to the device and eliminates the magnetic energy stored within the film.

III. CONCLUSION

In this article, we investigated the inductance properties of YBCO single and multilayer films grown commercially on large area wafers with thickness less than the penetration depth. The presence of a superconducting ground plane in the multilayer film substantially reduces the geometric component of the sheet inductance. This significantly relaxes circuit design constraints for single flux quanta device components requiring small inductance such as adiabatic quantum flux paramtrons [26]. Furthermore, we showed that the ground plane can serve as an environmental magnetic shielding layer for SQUID devices. This could aid SQUID [27], [28] or Josephson array [29] based applications for magnetically noisy environments.

ACKNOWLEDGMENT

The authors would like to thank R. Semerad of Ceraco GMBH for the development of the multilayer structure.

REFERENCES

- [1] H. Wakana, "Improvement in reproducibility of multilayer and junction process for HTS SFQ circuits," *IEEE Trans. Appl. Supercond.*, vol. 15, no. 2, pp. 153–156, Jun. 2005.
- [2] T. Wolf *et al.*, "YBCO Josephson junctions and striplines for RSFQ circuits made by Ion irradiation," *IEEE Trans. Appl. Supercond.*, vol. 23, no. 2, Apr. 2013, Art. no. 1101205.
- [3] S. K. Tolpygo *et al.*, "Advanced fabrication processes for superconducting very large-scale integrated circuits," *IEEE Trans. Appl. Supercond.*, vol. 26, no. 3, Apr. 2016, Art. no. 1100110.
- [4] S. A. Cybart *et al.*, "Nano Josephson superconducting tunnel junctions in $\text{YBa}_2\text{Cu}_3\text{O}_{7-\delta}$ directly patterned with a focused helium ion beam," *Nature Nanotechnol.*, vol. 10, pp. 598–602, Jul. 2015.
- [5] L. Kasaei *et al.*, "MgB₂ Josephson junctions produced by focused helium ion beam irradiation," *AIP Adv.*, vol. 8, no. 7, Jul. 2018, Art. no. 075020.
- [6] B. Müller *et al.*, "Josephson junctions and SQUIDs created by focused helium-Ion-beam irradiation of $\text{YBa}_2\text{Cu}_3\text{O}_{7-\delta}$," *Phys. Rev. Appl.*, vol. 11, no. 4, Apr. 2019, Art. no. 044082.
- [7] F. Couédo *et al.*, "Dynamic properties of high- T_c superconducting nano-junctions made with a focused helium ion beam," Aug. 2019, *arXiv:1908.11163*.
- [8] G. D. Martinez, D. Buckley, I. Charaev, A. Dane, D. E. Dow, and K. K. Berggren, "Superconducting nanowire fabrication on niobium nitride using helium ion irradiation," Mar. 2020, *arXiv:2003.02898*.
- [9] S. A. Cybart, K. Chen, and R. C. Dynes, "Planar $\text{YBa}_2\text{Cu}_3\text{O}_{7-\delta}$ Ion damage Josephson junctions and arrays," *IEEE Trans. Appl. Supercond.*, vol. 15, no. 2, pp. 241–244, Jun. 2005.
- [10] E. Y. Cho *et al.*, "YBa₂Cu₃O_{7- δ} superconducting quantum interference devices with metallic to insulating barriers written with a focused helium ion beam," *Appl. Phys. Lett.*, vol. 106, no. 25, Jun. 2015, Art. no. 252601.
- [11] H. Wakana *et al.*, "Ramp-edge junctions with interface-modified barriers fabricated on YBCO thick films," *IEEE Trans. Appl. Supercond.*, vol. 13, no. 2, pp. 595–598, Jul. 2003.
- [12] M. G. Forrester, A. Davidson, J. Talvacchio, J. R. Gavaler, and J. X. Przybysz, "Inductance measurements in multilevel high T_c step-edge grain boundary SQUIDS," *Appl. Phys. Lett.*, vol. 65, no. 14, Oct. 1994, Art. no. 1835.
- [13] H. Terai, M. Hidaka, T. Satoh, and S. Tahara, "Direct-injection high- T_c dc-SQUID with an upper $\text{YBa}_2\text{Cu}_3\text{O}_{7-x}$ ground plane," *Appl. Phys. Lett.*, vol. 70, no. 20, pp. 2690–2692, May 1997.
- [14] Y. Soutome, T. Fukazawa, K. Saitoh, A. Tsukamoto, and K. Takagi, "A YBCO multilayer process using surface-modified junction technology," *IEEE Trans. Appl. Supercond.*, vol. 13, no. 2, pp. 591–594, Jun. 2003.
- [15] P. Berberich, W. Assmann, W. Prusseit, B. Utz, and H. Kinder, "Large area deposition of YBa₂Cu₃O₇ films by thermal co-evaporation," *J. Alloys Compounds*, vol. 195, pp. 271–274, May 1993.
- [16] Y. T. Wang *et al.*, "YBa₂Cu₃O_{7- δ} - CeO₂ - YBa₂Cu₃O_{7- δ} multilayers grown by reactive co-evaporation on sapphire wafers," *IEEE Trans. Appl. Supercond.*, vol. 29, no. 5, Feb. 2019, Art. no. 1100804.
- [17] J. Clarke and A. I. Braginski, *The SQUID Handbook Applications of SQUIDs and SQUID Systems*, vol. 2. Hoboken, NJ, USA: Wiley, 2006.
- [18] H. Li, E. Y. Cho, H. Cai, Y. T. Wang, S. J. McCoy, and S. A. Cybart, "Inductance investigation of YBa₂Cu₃O_{7- δ} nano-slit SQUIDs fabricated with a focused helium ion beam," *IEEE Trans. Appl. Supercond.*, vol. 29, no. 5, Aug. 2019, Art. no. 1600404.
- [19] E. Y. Cho, H. Li, J. C. LeFebvre, Y. W. Zhou, R. C. Dynes, and S. A. Cybart, "Direct-coupled micro-magnetometer with Y-Ba-Cu-O nano-slit SQUID fabricated with a focused helium ion beam," *Appl. Phys. Lett.*, vol. 113, Oct. 2018, Art. no. 162602.
- [20] E. Y. Cho, Y. W. Zhou, J. Y. Cho, and S. A. Cybart, "Superconducting nano Josephson junctions patterned with a focused helium ion beam," *Appl. Phys. Lett.*, vol. 113, Jul. 2018, Art. no. 022604.
- [21] M. Prohämmer and J. P. Carbotte, "London penetration depth of d-wave superconductors," *Phys. Rev. B*, vol. 43, no. 7, Mar. 1991, Art. no. 5370.
- [22] J. E. Hirsch and F. Marsiglio, "London penetration depth in hole superconductivity," *Phys. Rev. B*, vol. 45, no. 9, Mar. 1992, Art. no. 4807.
- [23] Y. S. Barash, M. S. Kalenkov, and J. Kurkijärvi, "Low-temperature magnetic penetration depth in d-wave superconductors: Zero-energy bound state and impurity effects," *Phys. Rev. B*, vol. 62, no. 10, Sep. 2000, Art. no. 6665.
- [24] R. Meservey and P. M. Tedrow, "Measurements of the kinetic inductance of superconducting linear structures," *J. Appl. Phys.*, vol. 40, no. 5, Apr. 1969, Art. no. 2028.
- [25] A. T. Fiory, A. F. Hebard, P. M. Mankiewich, and R. E. Howard, "Penetration depths of high T_c films measured by two coil mutual inductances," *Appl. Phys. Lett.*, vol. 52, no. 25, Jun. 1988, Art. no. 2165.

- [26] N. Takeuchi, D. Ozawa, Y. Yamanashi, and N. Yoshikawa, "An adiabatic quantum flux parametron as an ultra-low-power logic device," *Supercond. Sci. Technol.*, vol. 26, no. 3, Jan. 2013, Art. no. 035010.
- [27] S. A. Cybart, S. M. Anton, S. M. Wu, J. Clarke, and R. C. Dynes, "Very large scale integration of nanopatterned $\text{YBa}_2\text{Cu}_3\text{O}_{7-\delta}$ Josephson junctions in a two-dimensional array," *Nano Lett.*, vol. 9, no. 10, pp. 3581–3585, Sep. 2009.
- [28] B. J. Taylor, S. A. Berggren, M. C. O'Brien, M. C. deAndrade, B. A. Higa, and A. L. de Escobar, "Characterization of large two-dimensional $\text{YBa}_2\text{Cu}_3\text{O}_{7-\delta}$ SQUID arrays," *Supercond. Sci. Technol.*, vol. 29, no. 8, Jun. 2016, Art no. 084003.
- [29] J. C. LeFebvre, E. Cho, H. Li, K. Pratt, and S. A. Cybart, "Series arrays of planar long Josephson junctions for high dynamic range magnetic flux detection," *AIP Adv.*, vol. 9, no. 10, Oct. 2019, Art. no. 105215.

Han Cai received the B.S. degree in optical and electronic information from the Huazhong University of Science and Technology, Wuhan, China, in 2012, the M.S. degree in physics from Tohoku University, Sendai, Japan, in 2015, and the M.E. degree in electrical engineering from Tsinghua University, Beijing, China, in 2017. She is currently working toward the Ph.D. degree in electrical engineering with the University of California Riverside, Riverside, CA, USA.

Her research interests include superconducting digital circuit and quantum computing.

Hao Li received the B.S. degree in microelectronics from Jilin University, Changchun, China, in 2010, and the Ph.D. degree in electrical engineering from Tsinghua University, Beijing, China, in 2017.

He is currently a Postdoctoral Researcher with the Department of Electrical and Computer Engineering, University of California, Riverside, Riverside, CA, USA. His research interests include reversible computing, quantum computing realized by low- T_C superconducting electronics, and high- T_C superconducting devices fabricated by focused helium ion beam direct-writing.

Ethan Y. Cho was born in Philadelphia, PA, USA, in 1986. He received the B.S. degree in physics from Nation Tsing Hua University, Hsinchu, Taiwan, in 2009 and the Ph.D. degree in physics from the University of California, San Diego, San Diego, CA, USA, in 2016.

His research interest includes high critical temperature superconductor physics, superconducting electronics 2-D Josephson junction array, superconducting digital circuits, and He-FIB nano fabrication.

Shane A. Cybart (Senior Member, IEEE) received the Ph.D. degree in materials science and engineering from the University of California, San Diego (UC San Diego), San Diego, CA, USA, in 2005.

He is currently an Assistant Professor of Electrical and Computer Engineering with the University of California, Riverside, Riverside, CA, USA. After working as a Postdoctoral Scholar with the Department of Physics, University of California, Berkeley (UC Berkeley) from 2006 to 2009. Afterward he worked as a Project Scientist with UC Berkeley/LBNL from 2009 to 2013 and UC San Diego from 2013 to 2016. In 2016, he was appointed as an Assistant Professor with the UC Riverside, where he currently leads the Oxide Nano Electronics Lab. His research interests focus on high-critical-temperature superconducting materials, devices, and nano-fabricated circuits using focused helium ion beam (He-FIB) techniques. Research areas include high transition temperature superconducting electronics, Josephson junction arrays, and superconducting digital circuits.